Assessing the oxidation states and structural stability of the Ce analogue of brannerite

Esther Rani Aluri, Lisa M. Bachiu, Andrew P. Grosvenor*
Department of Chemistry, University of Saskatchewan, Saskatoon, SK Canada

Scott H. Forbes, John E. Greedan
Department of Chemistry & Chemical Biology, McMaster University, Hamilton, ON Canada

* Author to whom correspondence should be addressed
E-mail: andrew.grosvenor@usask.ca
Phone: (306) 966-4660
Fax: (306) 966-4730

Abstract:

The Ce-containing analogue of brannerite (i.e., UTi_2O_6) was previously considered to be stoichiometric (i.e., $CeTi_2O_6$); however, it has recently been determined that the material is O deficient. This oxygen deficient material has been suggested to be charged balanced by the presence of a minor concentration of Ce^{3+} or by the A-site being cation deficient with the Ce oxidation state being 4+. A variety of Ti-containing oxides (including brannerite) have been investigated as potential nuclear wasteforms and it is necessary to understand the electronic structure of a proposed nuclear wasteform material as well as how the structure responds to radiation from incorporated waste elements. The radiation resistance of a material can be simulated by ion implantation. The objective of this study was to confirm the Ce oxidation state in the cation and oxygen deficient material (i.e., $Ce_{0.94}Ti_2O_{6-\delta}$) and to determine how radiation damage affects this material. X-ray Photoelectron Spectroscopy (XPS) and X-ray Absorption Near-edge Spectroscopy (XANES) were used to study $Ce_{0.94}Ti_2O_{6-\delta}$ before and after being implanted with 2 MeV Au^- ions. Analysis of the Ce 3d XPS spectra from the as-synthesized samples using a previously developed fitting method has unequivocally shown that Ce adopts both 4+ (major) and 3+ (minor) oxidation states, which was confirmed by examination of magnetic susceptibility data. Analysis of XPS and XANES spectra from ion implanted materials showed that both Ce and Ti were reduced as a result of radiation damage and that the local coordination environments of the cations are greatly affected by radiation damage.

Keywords: Nuclear wasteform, Brannerite, XPS, XANES, Ion implantation, XRD, Magnetic susceptibility

1. Introduction:

One proposal for dealing with nuclear waste, particularly spent nuclear fuel, is to contain the waste elements (fission products and actinides) within the crystal structures of a series of metal oxides. SYNROC (synthetic rock), which contains metal oxides adopting the zirconolite, hollandite, perovskite, and rutile structures, was developed for this application.[1,2,5,6] The majority of the materials present in SYNROC are Ti-based oxides, as a result of the ability of these materials to incorporate a wide range of waste elements in the structures that they adopt and the generally improved corrosion resistance of these materials.[1-9] Other Ti-based mineral structures have also received attention as potential nuclear wasteforms, including the brannerite structure.[3-8] The brannerite mineral (UTi_2O_6) has received attention from the nuclear wasteform research community owing to the ability of this mineral to incorporate a significant amount of U (~55 wt%).[6] The monoclinic structure of brannerite (UTi_2O_6; space group C2/m) is presented in **Fig. 1**. The structure is built-up of alternating columns of UO_6 octahedra and layers of TiO_6 octahedra with the U-containing layer being half as dense as the Ti-containing layer.[7,8] Chains of edge-sharing UO_6 octahedra form along the b-axis. The edge-sharing TiO_6 octahedra form a zigzag layer in the a/b plane and are corner sharing with the UO_6 octahedra along the c-axis.[7,8] The UO_6 octahedra are regular in shape while the TiO_6 octahedra are distorted in a similar fashion to those present in the anatase structure of TiO_2.[7,8] The Ce-containing analogue of this material has been investigated for many years owing to the ease associated with dealing with a rare-earth containing material compared to an actinide containing material.

The Ce analogue of brannerite has been considered to be a stoichiometric material for many years (i.e., $CeTi_2O_6$); however, this has been called into question.[10-12] Recent studies have suggested that this material is, in fact, oxygen deficient. (Either the ceramic method or a soft chemistry method followed by high-temperature annealing was used to produce the materials studied in these separate studies.[10-12]) Two reasons for the observed oxygen deficiency have been proposed in the literature. One proposal is that Ce has a mixture of oxidation states (3+ and 4+) with the ratio of these oxidation states varying depending on the way in which the materials are cooled after high-temperature synthesis because of the temperature dependant Ce^{3+}/Ce^{4+} reduction-oxidation couple.[10]

An alternate proposal that has been presented to explain the oxygen deficiency is that the material is Ce deficient, which would require that it also be O deficient so as to be charged balanced.[11,12] This second proposal has also indicated that the Ce oxidation state is fixed at 4+.[11,12] All of the studies discussed above used (X-ray or neutron) diffraction and X-ray absorption near-edge spectroscopy (XANES) to study this material but have yielded conflicting results.[10-12] One objective of this study has been to resolve this issue.

When selecting a material for use as a nuclear wasteform, it is important to understand how it behaves upon exposure to radiation from incorporated waste elements undergoing radioactive decay. Natural brannerite mineral samples (i.e., UTi_2O_6) are often found to be metamict (amorphous) because of accumulated radiation damage, which may limit the usefulness of this material as a nuclear wasteform.[11] This being noted, studies of brannerite analogues are of interest owing to the concentration of U that is found in the natural mineral.[6] Limited information is available on the radiation tolerance of the Ce analogue of brannerite and it is necessary to understand the behaviour of this material upon exposure to radiation so as to determine if it behaves in a similar fashion to UTi_2O_6. Studying the effect of radiation-induced structural damage on materials containing an internal radiation source (e.g., Pu- or Am-substituted materials) can be difficult for a variety of reasons including: safety, availability of the radioactive element, and the ability to study these materials using a variety of techniques. These hurdles can be overcome by using simulator elements (e.g., Ce, Zr, Gd) that mimic the chemistry of actinides and ion implantation using high-energy ion beams to study how radioactive decay damages a material.[9,13-15] It should be recognized that although ion implantation studies do allow for the investigation of how the structure of a material is affected by radiation damage, they do not (normally) allow for a study of how the daughter products produced during radioactive decay are incorporated with the material.

The objectives of this investigation have been to resolve the question regarding the oxidation state of Ce in $Ce_{1-x}Ti_2O_{6-\delta}$ and to understand how the structure of this material is affected by radiation. The nominal formula for $Ce_{1-x}Ti_2O_{6-\delta}$ has been suggested to be $Ce_{0.975}Ti_2O_{6-\delta}$, with the oxygen stoichiometry (i.e., 6-δ) assumed to be 5.95 based on a fixed Ce oxidation state of 4+.[11] In this study, a composition having the

formula unit of $Ce_{0.94}Ti_2O_{6-\delta}$ was investigated to insure that all of the Ce was incorporated within the brannerite structure with a trace amount of unreacted TiO_2 being present. The material, once synthesized, was annealed at temperatures lower than the synthesis temperature or slow-cooled to room temperature to study the effect of temperature on the average oxidation state of Ce. Materials were also exposed to high-energy Au^- ions to investigate how the structure responds to radiation. X-ray photoelectron spectroscopy (XPS) and XANES have been employed in this study to determine the average Ce oxidation state and to determine how the local structure of the ions that make up this material is affected by radiation induced damage. The results of these studies have been confirmed by the examination of powder X-ray diffraction (XRD) patterns and the collection of magnetic susceptibility data. It has been shown in this study that: (1) the average Ce oxidation state is <4+ in the Ce analogue of brannerite; (2) the average Ce oxidation state increased when the material was exposed to lower temperatures after high-temperature annealing; and (3) that radiation induced damage affects the coordination environment of the ions within the material and results in the partial reduction of both Ce and Ti.

2. Experimental:

2.1. Synthesis and powder X-ray diffraction:

The material studied (i.e., $Ce_{0.94}Ti_2O_{6-\delta}$) was prepared using the ceramic method. Three sets of samples containing a mixture of CeO_2 (Alfa Aesar; 99.9%) and TiO_2 (Alfa Aesar; >99%) having a 0.94:2 (CeO_2:TiO_2) molar ratio were ground using a mortar and pestle and formed into pellets using a pellet press and pressure of 6 MPa. Each pellet was placed in a tube furnace set to 600 ^oC and heated to 1325 ^oC over 8 hrs followed by a soak at 1325 ^oC (in air) for 3 days, at which point the pellets were quench cooled in air, ground, pelleted and reheated in the same manner as before for another 3 days before quench cooling. After checking that the reactants had reacted as fully as possible by powder XRD using a Panalytical Empyrean instrument, some samples were ground and pelleted for further heat treatments. One set of samples was annealed at 800 ^oC for 40 hrs followed by being quench cooled in air while another set of samples was first heated at 1325 ^oC for 1 day followed by slow cooling to room temperature (RT) over a period of ~3 days. In total, three sets of samples were produced: one that was quenched cooled

from 1325 °C to room temperature in air; one that was annealed at 800 °C after reaction at 1325 °C; and one that was cooled slowly to RT from 1325 °C. In agreement with previously reported results, each set of materials showed different colours after cooling.[10] The samples that were quench cooled from 1325 °C were dark brown in colour while the samples that were annealed at 800 °C or slow-cooled to RT were yellow in colour (see **Fig. 2**). The observed differences in colour have previously been ascribed to changes in the average Ce oxidation state depending on the method used to cool the materials.[10]

High quality powder X-ray diffraction patterns were collected from representative samples using a PANalytical X'Pert Pro powder XRD equipped with a monochromatic Cu $K\alpha_1$ X-ray source. The powder XRD patterns were analysed by performing a Rietveld analysis using FullProf.[16]

2.2. Ion implantation:

The as-synthesized (i.e., quench cooled from 1325 °C) and slow-cooled samples of $Ce_{0.94}Ti_2O_{6-\delta}$ were implanted with 2 MeV Au^- ions using the 1.7 MeV Tandetron accelerator located at Interface Science Western (ISW), the University of Western Ontario. Sintered pellets of the $Ce_{0.94}Ti_2O_{6-\delta}$ materials were implanted at room temperature with 2 MeV Au^- ions to a dose of 5×10^{14} ions/cm^2. The ion beam was aligned normal to the pellet surface during implantation. Profiles of the ion implantation depth and the number of vacancies produced per Au^- ion per nm were calculated using the Stopping and Range of Ions in Matter (SRIM-2013) software package.[17] The ions were calculated to penetrate to a maximum depth of ~800 nm.

2.3. XPS analysis:

The XPS spectra from the $Ce_{0.94}Ti_2O_{6-\delta}$ samples were collected using a Kratos AXIS Ultra XPS instrument equipped with a monochromatic Al Kα X-ray (1487 eV) source that is located at Surface Science Western (SSW), the University of Western Ontario. Finely powdered samples of the as-synthesized materials were studied along with the ion-implanted pellets. Survey spectra were collected using a pass energy of 160 eV, a step size of 0.7 eV, and an energy window of 1100 – 0 eV. High resolution Ce 3d, O 1, Ti 2p, and C 1s spectra were collected using a pass energy of 20 eV, a step size of 0.05 eV, and an appropriately sized energy window. All spectra were collected with the

charge neutralizer turned on and were calibrated by setting the C 1s binding energy (BE) of adventitious C observed in the C 1s spectra from each sample to 284.8 eV. The XPS spectra were analysed using CasaXPS.[18]

2.4. XANES analysis:

The Ce L_3- and Ti K-edge XANES spectra were collected using the Canadian Light Source/X-ray Science Division Collaborative Access Team (CLS@APS, Sector 20) bending magnetic beamline (20BM) located at the Advanced Photon Source (APS), Argonne National Laboratory and the Soft X-ray Microcharacterization Beamline (SXRMB, 06B1-1) located at the Canadian Light Source (CLS).[19,20] Both beamlines employed Si (111) monochromators and provided spectra having similar resolutions. Spectra were collected from finely ground powders deposited on C tape (SXRMB) or sealed between layers of Kapton tape (20BM), and were collected in total electron yield (TEY; SXRMB), transmission (20BM), and/or partial fluorescence yield (PFY; SXRMB and 20BM) modes. All spectra were collected using an energy step size of 0.15 eV/step through the absorption edge. The Ti K-edge spectra were calibrated using Ti metal (4966 eV) and the Ce L_3-edge spectra were calibrated using Cr metal (5989 eV).

XANES spectra were also collected from the ion-implanted pellets using the SXRMB and 20BM beamlines so as to study the effect of radiation damage on the local structure of the $Ce_{0.94}Ti_2O_{6-\delta}$ materials. Spectra were collected in PFY and/or TEY mode using an energy step size of 0.15 eV/step through the absorption edge. The Ce L_3-edge XANES spectra collected in PFY mode from the ion implanted materials were severely affected by absorption effects, so only the TEY Ce L_3-edge XANES spectra are reported. Absorption effects did not affect the Ti K-edge XANES spectra collected in PFY mode. All XANES spectra discussed in this contribution were analysed using the Athena software program.[21]

2.5. Magnetic Susceptibility:

Magnetization data were collected on a powdered sample of $Ce_{0.94}Ti_2O_{6-\delta}$ using a Magnetic Property Measurement System (MPMS) from Quantum Design. The applied field was 0.1 T and data were taken over the temperature range of 4 K (-269.15 ^oC) to 300 K (26.85 ^oC) in both field cooled (FC) and zero field cooled (ZFC) modes. Susceptibility data were obtained by dividing the measured magnetic moment by the

applied field. Diamagnetic corrections were applied to the data using standard literature values.[22]

3. Results and Discussion:

3.1. XRD analysis of as-synthesized materials:

Powder XRD patterns were collected from all materials studied to confirm the presence of brannerite. Representative powder XRD patterns from $Ce_{0.94}Ti_2O_{6-\delta}$ quench cooled from 1325 ^oC or slow cooled to RT are presented in **Fig. 3** along with the results of the Rietveld refinement of the pattern associated with the brannerite structure, which are also presented in **Table 1**. All patterns were observed to primarily contain the Ce analogue of brannerite along with a minor concentration of TiO_2. This observation is consistent with the stoichiometry used to form these materials (i.e., $Ce_{0.94}Ti_2O_{6-\delta}$), as it has been determined previously that $Ce_{0.975}Ti_2O_{6-\delta}$ is the most likely composition for this material.[11] A slight excess of TiO_2 was purposefully used during the synthesis of these materials to make sure that no CeO_2 remained after heating, as the focus of this study was to identify how the Ce oxidation state changes in brannerite depending on the cooling method used after high-temperature annealing. The results of the Rietveld refinements (**Fig. 3 and Table 1**) are consistent with previously reported results for these materials.[11,12]

3.2. XANES and XPS analysis of the as-synthesized materials:

3.2.1. Ce L_3-edge XANES spectra:

Ce L_3-edge XANES spectra were collected from the as-synthesized brannerite materials (**Fig. 4a**) and result from the excitation of 2p electrons to 5d states with the lineshape of the spectrum from Ce^{3+} being considerably different than the spectrum from Ce^{4+}.[23-25] Four features are observed in spectra from Ce^{4+}-containing materials (labelled as B_1, B_2, B_3, and B_4 in **Fig. 4a**) because of a pre-edge, quadrupolar 2p → 4f transition (B_1), and three dipolar, 2p → 5d transitions resulting from changes in the Ce 4f final-state occupancies ($4f^2$ (B_2), $4f^1$ (B_3), and $4f^0$ (B_4)).[24,25] The excitation of a 2p electron from Ce^{3+} results in the observation of only one intense peak in the Ce L_3-edge spectrum and has a similar energy to feature B_2 in the spectrum from Ce^{4+}.[10]

The spectral lineshapes observed in **Fig. 4a** have been used in the past to argue for the presence of only Ce^{4+} in these materials owing to the similarity of these spectra to

those from materials that exclusively contain Ce^{4+}.[11,12] However, closer inspection of the spectra shows that there is a slight difference in the intensity of feature B_2 when comparing the material quench cooled from 1325 ^oC vs. the material that was slow-cooled to RT after high-temperature annealing (**Fig. 4a**). It is argued here that this difference is a result of the presence of more Ce^{3+} in the quench cooled sample. A linear combination fitting was performed on the spectrum from the quench cooled sample using $CePO_4$ (Ce^{3+}) and the slow-cooled $Ce_{0.94}Ti_2O_{6-\delta}$ sample as standards. As is shown in **Fig. 4b**, the spectrum from the quench cooled sample is reproduced when a combination of the two standard spectra are used that contains ~7% of the Ce^{3+} standard. It should be noted that this analysis only provides the relative difference in the [Ce^{3+}] between the two samples and not the absolute [Ce^{3+}] in each sample.

3.2.2. Ce 3d XPS spectra:

It has been demonstrated previously that both Ce $M_{4,5}$-edge XANES spectra and Ce 3d XPS spectra, which both result from the excitation of Ce 3d electrons, are highly sensitive to changes in the Ce oxidation state.[10,26] This increased sensitivity is a result of the greater resolution of these spectra compared to the resolution of Ce L_3-edge XANES spectra. Ce 3d XPS spectra have been collected in the present study to better understand the oxidation state of Ce in the as-synthesized brannerite materials and to settle the question regarding the presence of Ce^{3+} in these materials. Ce 3d XPS spectra from $CePO_4$ and CeO_2 are presented in **Fig. 5** to show the significant spectral differences observed when studying Ce^{3+}- or Ce^{4+}-containing materials. The reasons for the different features present in the spectra have been discussed in detail previously along with the method used to fit these spectra (see **Fig. 5**); however, a short description is provided here.[26] Eight peaks were used to fit the spectrum from CeO_2, which may also contain traces of Ce^{3+} as a result of surface defects. The multiple components representing the spin-orbit split peaks result from the different Ce 4f occupancies in the final state ($4f^{0,1,2}$) along with the presence of satellite peaks.[27] The Ce 3d XPS spectrum from $CePO_4$, however, only contains two pairs of spin-orbit split peaks. The spectra have been fitted with pairs of peaks with the lowest binding energy peak representing the core-line and the corresponding higher binding energy peak representing a shake-up satellite peak. The Ce $3d_{5/2}$ components have been labeled as v and u, referring to the Ce^{4+} and Ce^{3+}

components, respectively, while the Ce $3d_{3/2}$ components have been labeled as v' and u'. The integrated peak areas of the fitted component peaks were used to calculate the relative [Ce^{3+}] in the brannerite samples.[28] The spectra presented in **Fig. 5** are consistent with those reported previously.[26]

The Ce 3d XPS spectra from the three $Ce_{0.94}Ti_2O_{6-\delta}$ materials studied here are presented in **Fig. 6** and were fitted to determine if Ce^{3+} was present. When compared to the spectra presented in **Fig. 5**, it can be seen that the spectra from $Ce_{0.94}Ti_2O_{6-\delta}$ contain features representing Ce^{4+} (major) and Ce^{3+} (minor). The spectra were fitted using the method described above (and elsewhere) to determine the Ce^{3+}:Ce^{4+} ratios.[26] The results of the fittings are presented in **Table 2**. The $Ce_{0.94}Ti_2O_{6-\delta}$ sample that was analysed after being quench-cooled from 1325 ^oC was observed to contain the highest concentration of Ce^{3+} (~41% Ce^{3+}), followed by the sample that was quench-cooled and then post-annealed at 800 ^oC (~34% Ce^{3+}), and finally the sample that was slow-cooled to RT after high-temperature annealing at 1325 ^oC (~32% Ce^{3+}). The difference in the amount of Ce^{3+} present in the quech-cooled sample vs. the slow-cooled sample (~9% Ce^{3+}) is consistent with the linear combination fitting analysis of the Ce L_3-edge XANES spectra discussed above (~7% Ce^{3+}; cf. **Fig. 4**). This analysis confirms the previously reported conclusion that Ce^{3+} is present in the Ce-analogue of brannerite.[10]

3.2.3. Ti K-edge XANES spectra:

Examination of the Ce L_3-edge XANES and Ce 3d XPS spectra confirmed that the Ce-analogue of brannerite contains Ce^{3+} (along with Ce^{4+}), which would require the material to be O-deficient. As such, it would be expected that the average Ti coordination number (CN) would be less than the nominal value of 6 observed in the structure of the U-containing material (UTi_2O_6), and that the CN would change depending on how the material was cooled after high-temperature annealing.

Ti K-edge XANES spectra are sensitive to changes in Ti CN, and result from 1s→3d (pre-edge) and 1s→4p (main-edge) transitions, with the pre-edge region being particularly sensitive to changes in CN.[29-31] These XANES spectra follow dipole selection rules (i.e., $\Delta l = +/-1$); however, quadrupolar transitions (e.g., 1s→3d) can also be observed, although they are generally weak when compared to dipolar transitions (e.g., 1s→4p). As the CN decreases from 6, increased orbital overlap will occur between Ti 3d

and Ti 4p states, resulting in an increased dipolar character (and therefore intensity) of the of the pre-edge region.[29,31-33]

The Ti K-edge XANES spectra from $Ce_{0.94}Ti_2O_{6-\delta}$ quench-cooled from 1325 ^oC, annealed at 800 ^oC after high-temperature annealing, or slow-cooled to RT from 1325 ^oC are presented in **Fig. 7** with the appropriate excitations labelled. The Ti K-edge spectra from all three samples have lineshapes that would be expected for Ti^{4+} ions in a near 6-coordinate environment; however, the pre-edge peak intensities are greater than would be expected for Ti^{4+} in ordered 6-coordinate environments as a result of the distortion of the Ti-O coordination environment in the brannerite structure and the lower, average Ti CN as a result of the O-deficiency. What is clearly obvious from the spectra is the lack of differences observed between the spectra regardless of the method used to cool these materials. The differences in the Ce^{3+}:Ce^{4+} ratio present in the quench cooled sample vs. the slow cooled sample (**Table 2**) would result in an increased O-deficiency in the quench cooled sample compared to the other materials and a reduced, average Ti CN. *Stennett et al.* found through analysis of neutron powder diffraction data that the Ce cation deficiency in these materials is balanced by deficiency in the O site that connects the Ti-O and Ce-O coordination environments, which are both nominally 6-coordinate in the brannerite (UTi_2O_6) structure.[11] The lack of variation observed in the Ti K-edge XANES structure from the Ce analogue of brannerite when quench-cooled vs. annealing at lower temperatures after high-temperature heating may be explained by studying the structure.[10,11] Three non-equivalent O sites are present within the brannerite structure. Two of these sites contain O ions that interact with both Ce and Ti while the third site contains O ions located between Ti atoms within the zigzag layer of TiO_6 octahedra.[11,34] This later O site only coordinates to Ti atoms and accounts for three of the six O atoms in each TiO_6 octahedra.[34] As such, it appears that the changing O deficiency observed in these materials depending on cooling conditions does not significantly affect the average Ti CN, leading to the observation of very little change in the Ti K-edge XANES spectra despite the differences observed in the Ce 3d XPS and Ce L_3-edge XANES spectra. This being stated, higher resolution Ti K-edge (or Ti $L_{2,3}$-edge) XANES spectra may yield more insight.

3.3. Magnetic properties of the as-synthesized materials:

The Ce 3d XPS spectra collected from powders of the $Ce_{0.94}Ti_2O_{6-\delta}$ materials clearly indicated the presence of Ce^{3+} in these materials; however, one could argue that surface defects could be responsible for the presence of Ce^{3+} owing to the surface sensitivity of XPS, and that the calculated Ce^{3+} concentration does not properly reflect the true Ce^{3+} concentration present in the bulk material. This could also be proposed as the reason for why no variations in the Ti K-edge XANES spectra were observed. Magnetic susceptibility data were collected to confirm the presence of Ce^{3+} in the $Ce_{0.94}Ti_2O_{6-\delta}$ sample that was post-annealed at 800 ^oC after being synthesized at 1325 ^oC followed by quench cooling (see **Fig. 8**). The sample was observed to be strongly paramagnetic, which must be attributed to significant levels of Ce^{3+} being present in the bulk of the material. A plot of the inverse susceptibility (see inset in **Fig. 8**) shows a reasonable adherence to the Curie-Weiss law (Eq.1) above 220 K (-53.15 ^oC). The magnetic susceptibilities of Ce^{3+} compounds are strongly influenced by crystal field effects as the separation between the crystal field split states is of the order of ~100 K (-173.15 ^oC) and only at higher temperatures is the Curie-Weiss law obtained. The Curie constant (C) obtained from this fit is 0.285(3) (emu/mole)K. The expected C value would be 0.804 x 0.94 = 0.756 (emu/mole)K if all Ce cations present were Ce^{3+}. Thus, the atomic percent of Ce^{3+} in this sample is ~38%, which is in reasonable agreement with the value obtained from analysis of the Ce 3d XPS spectrum from this sample (~34% Ce^{3+}). Fits using slightly different temperature intervals gave similar values for C to within ~5%, which is a reasonable error to assign to the [Ce^{3+}] obtained by this particular method.

$$\chi = C/(T - \theta) \qquad \text{(Eq. 1)}$$

3.4. Examination of ion-implanted $Ce_{0.94}Ti_2O_{6-\delta}$:

The development of materials (crystalline or amorphous) for the safe sequestration of nuclear waste requires knowledge of how these (and related) materials will be affected by the radioactive decay of incorporated waste elements. The materials studied here were implanted with 2 MeV Au^- ions to a dose of 5 x 10^{14} ions/cm^2 followed

by XANES and XPS analysis to study if the procedure used to cool the materials influenced the response of these materials to radiation.

3.4.1. Ce 3d and Ti 2p XPS analysis:

XPS spectra were collected to understand how the surface chemistry of these materials was affected by ion implantation. The Ce 3d and Ti 2p XPS spectra from the $Ce_{0.94}Ti_2O_{6-\delta}$ materials that were slow-cooled to RT after annealing at 1325 ^oC are presented in **Fig. 9** and have been compared to the corresponding spectra from the as-synthesized material. Examination of the Ce 3d XPS spectrum from the ion-implanted material shows a clear difference in lineshape compared to the spectrum from the as-synthesized material, with the former spectrum more resembling that of Ce^{3+} than Ce^{4+} (cf. **Fig. 9a**). Fitting of the Ce 3d XPS spectrum from the ion-implanted material gives a Ce^{3+}:Ce^{4+} ratio of 69:31, which is significantly different than the ratio determined for the as-synthesized material (32:68). It is known that low energy (KeV) ion sputtering of Ce containing surfaces can result in the reduction of Ce^{4+} to Ce^{3+}, and the observation reported above was expected considering that the materials were implanted with 2 MeV Au^- ions.[35,36]

The Ti 2p XPS spectra from the ion implanted samples are presented in **Fig. 9b** and have been normalized to show the differences in linewidth between the spectra collected from the as-synthesized material vs. the ion-implanted material. Both spectra show $2p_{3/2}$ and $2p_{1/2}$ spin orbit split peaks that are relatively narrow owing to the lack of multiplet splitting observed in spectra that (primarily) contain Ti^{4+}. The binding energy of the Ti $2p_{3/2}$ peak in the spectrum from the as-synthesized material (458.2 eV) is in agreement with previously reported values for Ti^{4+}.[37] After ion-implantation, the resulting spectrum was found to be broader to lower binding energy (compared to the spectrum from the as-synthesized material), which is considered to be a result of the partial reduction of Ti. It was found that two peaks were required to properly fit each spin-orbit split feature in the Ti 2p XPS spectrum from the ion-implanted material (not shown), with the higher binding energy ($2p_{3/2}$ or $2p_{1/2}$) peak corresponding to Ti^{4+} and the lower binding energy ($2p_{3/2}$ or $2p_{1/2}$) peak corresponding to Ti^{3+}. The Ti^{4+}:Ti^{3+} ratio was observed to be ~82:18; however, this ratio changed considerably if the peak widths were allowed to vary.

3.4.2 Ce L_3- and Ti K-edge XANES analysis

The XPS spectra presented above only allowed for a study of how the surface regions of the pellets of these materials were affected by ion-implantation. Hard X-ray XANES spectra are inherently more bulk-sensitive than XPS spectra and are more sensitive to changes in the local coordination environments of the ions under investigation. Both Ti K-edge and Ce L_3-edge XANES spectra were collected from the ion-implanted pellets to study how ion implantation affected the sub-surface region of these materials, as well as the local coordination environment of Ti.

The Ce L_3-edge XANES spectrum from a pellet of $Ce_{0.94}Ti_2O_{6-\delta}$ that was slow-cooled to RT after annealing at 1325 ^oC followed by ion-implantation is presented in **Fig. 10** along with the spectrum from the as-synthesized material. The lineshape of the spectrum from the ion-implanted material is considerably different to the spectrum from the as-synthesized material and closely resembles previously reported spectra from CeO_x-TiO_2 materials that contained a significant concentration of Ce^{3+} (along with Ce^{4+}).[38] The identification of Ce^{3+} in the Ce L_3-edge XANES spectrum is in agreement with the analysis of the Ce 3d XPS spectra discussed in Section 3.4.1.

The Ti K-edge XANES spectra from the ion-implanted pellets of $Ce_{0.94}Ti_2O_{6-\delta}$ that were slow-cooled to RT after annealing at 1325 ^oC or quench-cooled in air from 1325 ^oC are presented in **Fig. 11** along with the spectrum the as-synthesized material (slow-cooled to RT after annealing at 1325 ^oC). In comparison to the as-synthesized material, the spectra from the ion-implanted materials show a decrease in energy and intensity of the main-edge region and an increase in the intensity of the pre-edge region. These changes are indicative of a decrease in the local coordination environment of the Ti ions as a result of disordering of the anion (and cation) lattice(s) during ion-implantation.[15,39] These spectral differences indicate that the brannerite structure is damaged by ion-implantation, which simulates the effect of decay of incorporated radioactive elements. It should be noted that little to no difference was observed between the Ti K-edge XANES spectra collected from the ion-implanted materials that received different cooling treatments and, therefore, contained different proportions of Ce^{3+} and Ce^{4+} (and O vacancies) prior to ion-implantation.

4. Conclusions

The study of the Ce analogue of brannerite has confirmed that this material is cation and anion deficient and that it contains both Ce^{3+} and Ce^{4+}. Further, it has been shown here that the Ce^{3+}:Ce^{4+} ratio in these materials varies depending on the way in which the materials are cooled post synthesis. Finally, examination of XPS and XANES spectra from the ion-implanted materials indicated that radioactive decay of incorporated nuclear waste elements will affect both the surface and sub-surface region of this material and that the method used to cool the materials did not appear to affect the response of this material to radiation. Although Ce is an insufficient analogue for U, it does behave in a very similar fashion to Pu, which can also exhibit an oxidation state of 3+.[8,23] Changes in the chemistry of these materials as a result of the decay of incorporated radioactive elements during nuclear waste sequestration could affect how they behave if exposed to aqueous environments. Future studies of these materials should examine how the leachability of these materials changes depending on the average Ce oxidation state.

Acknowledgements:

This project was funded by the Natural Sciences and Engineering Research Council (NSERC) of Canada through a Discovery grant awarded to APG. Mr. Jack Hendriks is thanked for carrying out the ion implantation studies using the Tandetron accelerator located at Interface Science Western, University of Western Ontario. Dr. Mark Biesinger is thanked for help in collection of the XPS spectra using the facilities located at Surface Science Western, University of Western Ontario. Dr. Paul Dube, Brockhouse Institute for Materials Research, McMaster University, is thanked for performing the magnetic susceptibility measurements. Dr. Zou Finfrock and Dr. Matthew Ward are thanked for their help in carrying out XANES measurements using the 20BM beamline (CLS@APS). The CLS@APS facilities are supported by the US Department of Energy-Basic Energy Sciences and the Canadian Light Source (CLS). Dr. Yongfeng Hu and Ms. Aimee Maclennan are thanked for their support in carrying out XANES experiments using the SXRMB (06B1-1) beamline located at the CLS. The CLS is supported by the Canada Foundation for Innovation, the Natural Sciences and Engineering Research Council, Western Economic Diversification Canada, the National Research Council of Canada, the Canadian Institutes of Health Research, the Government

of Saskatchewan, and the University of Saskatchewan. APG congratulates SSW on 35 year of performing excellent surface science research and education.

References:

[1] R. C. Ewing, W. J. Weber, F. W. Clinard Jr., *Prog. Nucl. Energy* **1995**; *29*, 63.

[2] A. E. Ringwood, S. E. Kesson, N. G. Ware, W. Hibberson, A. Major, *Nature* **1979**; *278*, 219.

[3] M. James, M. L. Carter, J. N. Watson, *J. Solid State Chem.* **2003**; *174,* 329.

[4] M. H. Donaldson, R. Stevens, B. E. Lang, J. Boerio-Goates, B. F. Woodfield, R. L. Putnam, A. Navrotsky, *J. Therm. Anal. Calorim.* **2005**; *81*, 617.

[5] J. Lian, L. M. Wang, G. R. Lumpkin, R. C. Ewing, *Nucl. Instrum. Methods Phys. Res., Sect. B* **2002**; *191*, 565.

[6] M. Colella, G. R. Lumpkin, Z. Zhang, E. C. Buck, K. L. Smith, *Phys. Chem. Minerals* **2005**; *32*, 52.

[7] G. R. Lumpkin, K. L. Smith, M. G. Blackford, *J. Nucl. Mater.* **2001**; *289*, 177.

[8] K. B. Helean, A. Navrotsky, G. R. Lumpkin, M. Colella, J. Lian, R. C. Ewing, B. Ebbinghaus, J. G. Catalano *J. Nucl. Mater.* **2003**; *320*, 231.

[9] R. C. Ewing, W. J. Weber, J. Lian *J. Appl. Phys.* **2004**; *95*, 5949.

[10] L. T. Huynh, S. B. Eger, J. D. S. Walker, J. R. Hayes, M. W. Gaultois, A. P. Grosvenor *Solid State Sci.* **2012**; *14*, 761.

[11] M. C. Stennett, C. L. Freeman, A. S. Gandy, N. C. Hyatt, *J. Solid State Chem.* **2012**; *192*, 172.

[12] L. Kong, D. J. Gregg, I. Karatchevtseva, Z. Zhang, M. G. Blackford, S. C. Middleburgh, G. R. Lumpkin, G. Triani *Inorg. Chem.* **2014**; *53*, 6561.

[13] J. Lian, K. B. Helean, B. J. Kennedy, L. M. Wang, A. Navrotsky, R. C. Ewing *J. Phys. Chem. B* **2006**; *110*, 2343.

[14] S. X. Wang, L. M. Wang, R. C. Ewing, G. S. Was, G. R. Lumpkin *Nucl. Instrum. Methods. Phys. Rec., Sect. B* **1999**; *148*, 704.

[15] E. R. Aluri, J. R. Hayes, J. D. S. Walker, A. P. Grosvenor *J. Phys. Chem. C* **2014**; *118*, 7910.

[16] J. Carvajal-Rodríguez *Physica B* **1993**; *192*, 55.

[17] J.F. Ziegler, J.P. Biersack, M.D. Ziegler, *SRIM (The Stopping and Range of Ions in Solids)-2013*, MD: USA, **2013**.

[18] N. Fairley, *CasaXPS, Version 2.3.16; Casa Software Ltd.*, Teighnmouth, Devon, U.K., **2003**. www.casaxps.com.

[19] S.M. Heald, D.L. Brewe, E.A. Stern, K.H. Kim, F.C. Brown, D.T. Jiang, E.D. Crozier, R.A. Gordon *J. Synchrotron Radiat.* **1999**; *6*, 347.

[20] Y. F. Hu, I. Coulthard, D. Chevrier, G. Wright, R. Igarashi, A. Stinikov, B. W. Yates, E. L. Hallin, T. K. Sham, R. Reininger *AIP Conf. Proc.* **2010**; *1234*, 343.

[21] B. Ravel, M. Newville *J. Synchrotron Radiat.* **2005**; *12*, 537.

[22] P.W. Selwood, *Magnetochemistry*, Interscience Publishers, New York, **1956**.

[23] C. Lopez, X. Deschanels, J.M. Bart, J.M. Boubals, C. Den Auwer, E. Simoni *J. Nucl. Mater.* **2003**; *312*, 76.

[24] P. Nachimuthu, W.-C. Shih, R.-S. Liu, L.-Y. Jang, J.-M. Chen *J. Solid State Chem.* **2000**; *149*, 408.

[25] A. Kotani, K.O. Kvashnina, S.M. Butorin, P. Glatzel *J. Electron. Spectrosc. Rel. Phenom.* **2001**; *184*, 210.

[26] M. N. Revoy, R. W. J. Scott, A. P. Grosvenor *J. Phys. Chem. C*, **2013**; *117*, 10095.

[27] G. Kaindl, G. K. Wertheim, G. Schmiester, E. V. Sampathkumaran *Phys. Rev. Lett.* **1987**; *58*, 606.

[28] F. Larachi, J. Pierre, A. Adnot, A. Bernis *Appl. Surf. Sci.* **2002**; *195*, 236.

[29] T. Yamamoto *X-Ray Spectrom.* **2008**; *37*, 572.

[30] L.A. Grunes *Phys. Rev. B* **1983**; *27*, 2111.

[31] M.W. Gaultois, A.P. Grosvenor *J. Mater. Chem.* **2011**; *21*, 1829.

[32] D. Cabaret, A. Bordage, A. Juhin, M. Arfaoui; E. Gaudry *Phys. Chem. Chem. Phys.* **2010**; *12*, 5619.

[33] F. Farges, G. E. Brown, J. J. Rehr *Phys. Rev. B* **1997**; *56*, 1809.

[34] J. T. Szymański, J. D. Scott *Can. Mineral.* **1982**; *20*, 271.

[35] A. Pfau, K. D. Schierbaum *Surf. Sci.* **1994**; *321*, 71.

[36] M. Krawczyk, M. Holdynski, W. Lisowski, J. W. Sobczak, A. Jablonski *Appl. Surf. Sci.* **2015**; *341*, 196.

[37] C. D. Wagner, A. V. NAumkin, A. Kraut-Vass, J. W. Allison, C. J. Powell, J. R. Rumble, Jr. *NIST Standard Reference Database, Version 3.4 (web version)*, htttp://srdata.nist.gov/xps/, **2003**.

[38] K. A. Michalow-Mauke, Y. Lu, K. Kowalski, T. Graule, M. Nachtegaal, O. Kröcher, D. Ferri *ACS Catal.* **2015**; *5*, 5657.

[39] E. R. Aluri, A. P. Grosvenor *J. Alloys Compd.* **2014**; *616*, 516.

Tables:

Table 1: Refined unit cell parameters for $Ce_{0.94}Ti_2O_{6-\delta}$ from the Rietveld analysis of powder XRD data

	$Ce_{0.94}Ti_2O_{6-\delta}$ Quench cooled	**$Ce_{0.94}Ti_2O_{6-\delta}$ Slow cooled to RT**
a (Å)	9.8266(2)	9.8308(2)
b (Å)	3.75253(7)	3.7550(1)
c (Å)	6.8849(1)	6.8979(2)
β (º)	119.2248(6)	119.2018(7)

Table 2: Ce^{4+} and C^{3+} concentrations in $Ce_{0.94}Ti_2O_{6-\delta}$ as determined by fitting of Ce 3d XPS spectra

	$Ce_{0.94}Ti_2O_{6-\delta}$ Quench cooled	**$Ce_{0.94}Ti_2O_{6-\delta}$ Annealed at 800 ^oC**	**$Ce_{0.94}Ti_2O_{6-\delta}$ Slow cooled to RT**
[Ce^{4+}]	59%	66%	68%
[Ce^{3+}]	41%	34%	32%

Figure captions:

Figure 1: A representation of the brannerite structure (UTi_2O_6) is shown looking down the b-axis.

Figure 2: An image showing how the colour of the Ce-analogue of brannerite varies depending on the cooling method used during the synthesis of the material is shown. The quench cooled sample is presented on the left while the sample that was slow cooled to RT is presented on the right.

Figure 3: The experimental powder XRD patterns and corresponding Rietveld refinement results are shown for (a) the quench cooled $Ce_{0.94}Ti_2O_{6-\delta}$ sample and (b) the $Ce_{0.94}Ti_2O_{6-\delta}$ sample that was slow cooled to RT.

Figure 4: The normalized Ce L_3-edge XANES spectra from samples that were either quench cooled or slow cooled to RT are presented in (a). The results of a linear combination fitting of the quench cooled sample is presented in (b) along with the weighed standard spectra used to fit this spectrum.

Figure 5: The fitted Ce 3d XPS spectra from (a) CeO_2 and (b) $CePO_4$ are shown.

Figure 6: The fitted Ce 3d XPS spectra from the $Ce_{0.94}Ti_2O_{6-\delta}$ materials that were (a) quench cooled from 1325 ^oC, (b) annealed at 800 ^oC followed by quench cooling, or (c) slow cooled from 1325 ^oC to RT are shown.

Figure 7: The Ti K-edge XANES spectra from the $Ce_{0.94}Ti_2O_{6-\delta}$ materials that were quench cooled from 1325 ^oC, annealed at 800 ^oC followed by quench cooling, or slow cooled from 1325 ^oC to RT are compared. The pre-edge (1s → 3d) and main-edge (1s → 4p) transitions are labelled.

Figure 8: The magnetic susceptibility of $Ce_{0.94}Ti_2O_{6.\delta}$ that was annealed at 800 ^oC post synthesis is shown. The inset shows a fit to the Curie-Weiss law (Eq. 1) above 200K. The small anomaly observed in the ZFC data near 50 K is due to the melting of solid O_2.

Figure 9: The (a) Ce 3d and (b) Ti 2p XPS spectra from the ion-implanted $Ce_{0.94}Ti_2O_{6-\delta}$ material that was slow cooled from 1325 ^oC to RT are shown and are compared to the corresponding spectra from the as-synthesized material.

Figure 10: The Ce L_3-edge XANES spectrum from the ion-implanted $Ce_{0.94}Ti_2O_{6-\delta}$ material that was slow cooled from 1325 ^oC to RT is shown and is compared to the corresponding spectrum from the as-synthesized material.

Figure 11: : The Ti K-edge XANES spectrum from the ion-implanted $Ce_{0.94}Ti_2O_{6-\delta}$ material that was slow cooled from 1325 ^oC to RT is shown and is compared to the corresponding spectrum from the as-synthesized material. The changes observed in the spectrum from the ion-implanted material when compared to the spectrum from the as-synthesized material are indicated by arrows. The observed increase in the pre-edge peak intensity and decrease in the energy and intensity of the main-edge features is indicative a decrease in the average local coordination number of Ti.

Figures:

Figure 1:

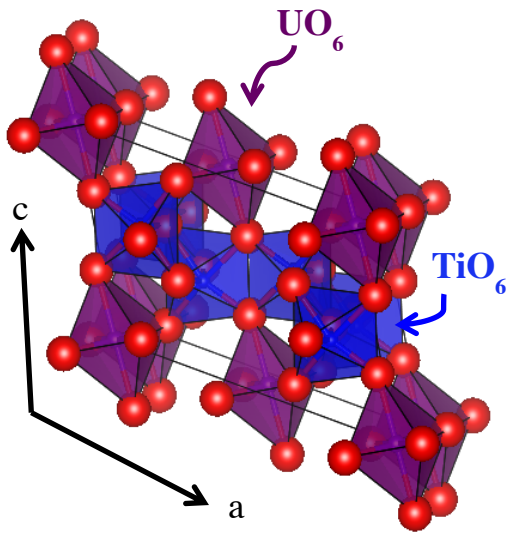

Figure 2:

Figure 3:

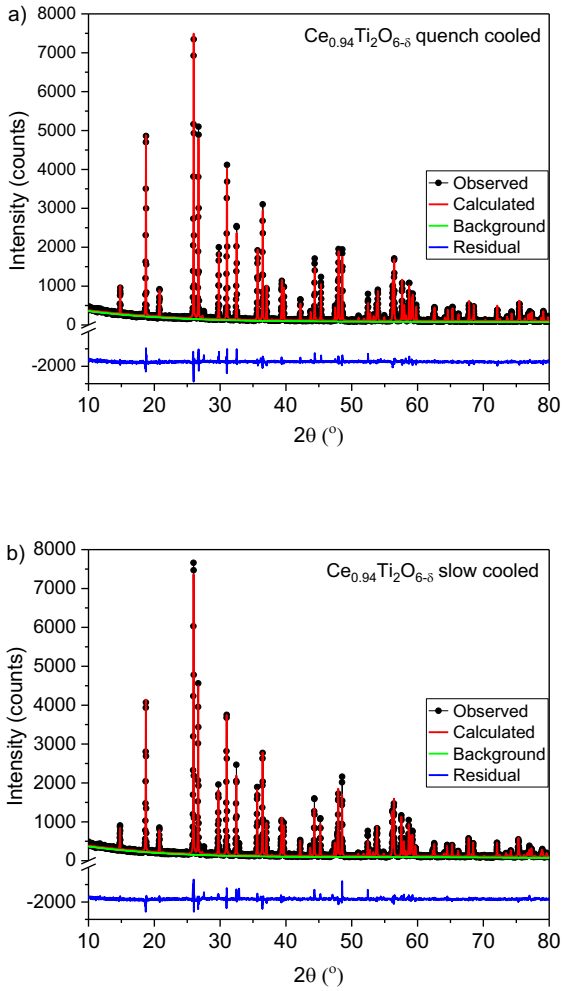
a)
$Ce_{0.94}Ti_2O_{6-\delta}$ quench cooled
Intensity (counts)
2θ (°)
Observed
Calculated
Background
Residual
b)
$Ce_{0.94}Ti_2O_{6-\delta}$ slow cooled
Intensity (counts)
2θ (°)
Observed
Calculated
Background
Residual

Figure 4:

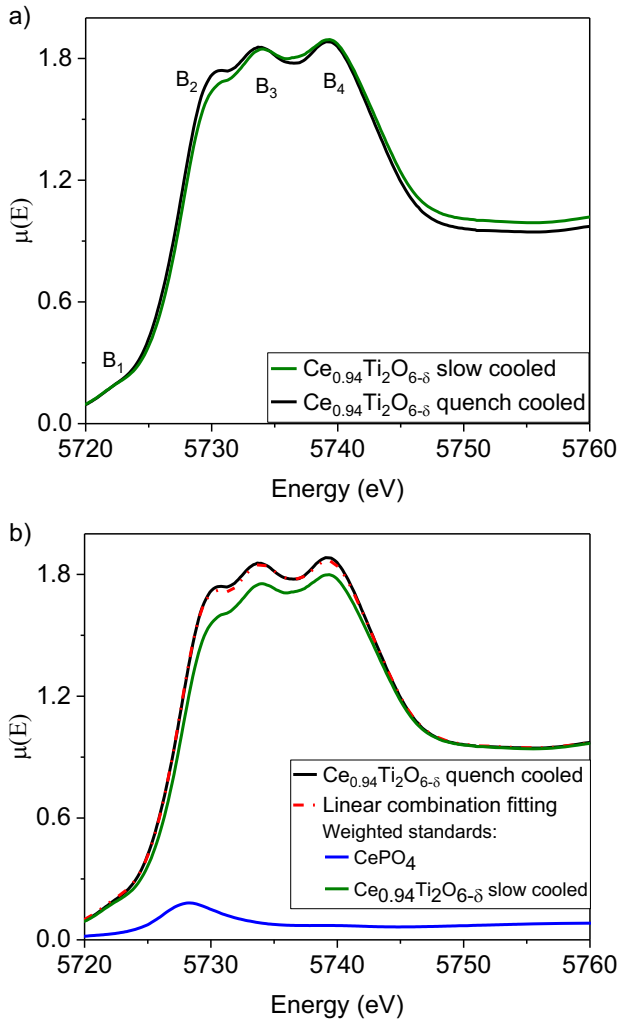
a)
1.8
1.2
0.6
0.0
μ(E)
B1
B2
B3
B4
Ce0.94Ti2O6-δ slow cooled
Ce0.94Ti2O6-δ quench cooled
5720
5730
5740
5750
5760
Energy (eV)
b)
1.8
1.2
0.6
0.0
μ(E)
Ce0.94Ti2O6-δ quench cooled
Linear combination fitting
Weighted standards:
CePO4
Ce0.94Ti2O6-δ slow cooled
5720
5730
5740
5750
5760
Energy (eV)

Figure 5:

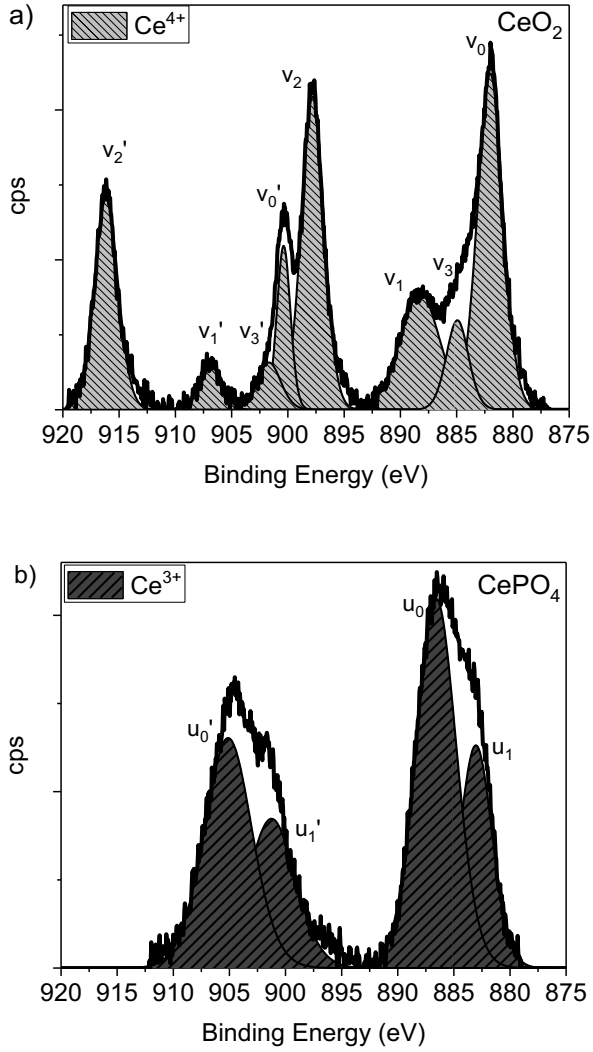
a)
Ce4+
CeO2
v0
v2
v2'
v0'
v1
v3
v1'
v3'
cps
920 915 910 905 900 895 890 885 880 875
Binding Energy (eV)
b)
Ce3+
CePO4
u0
u0'
u1
u1'
cps
920 915 910 905 900 895 890 885 880 875
Binding Energy (eV)

Figure 6:

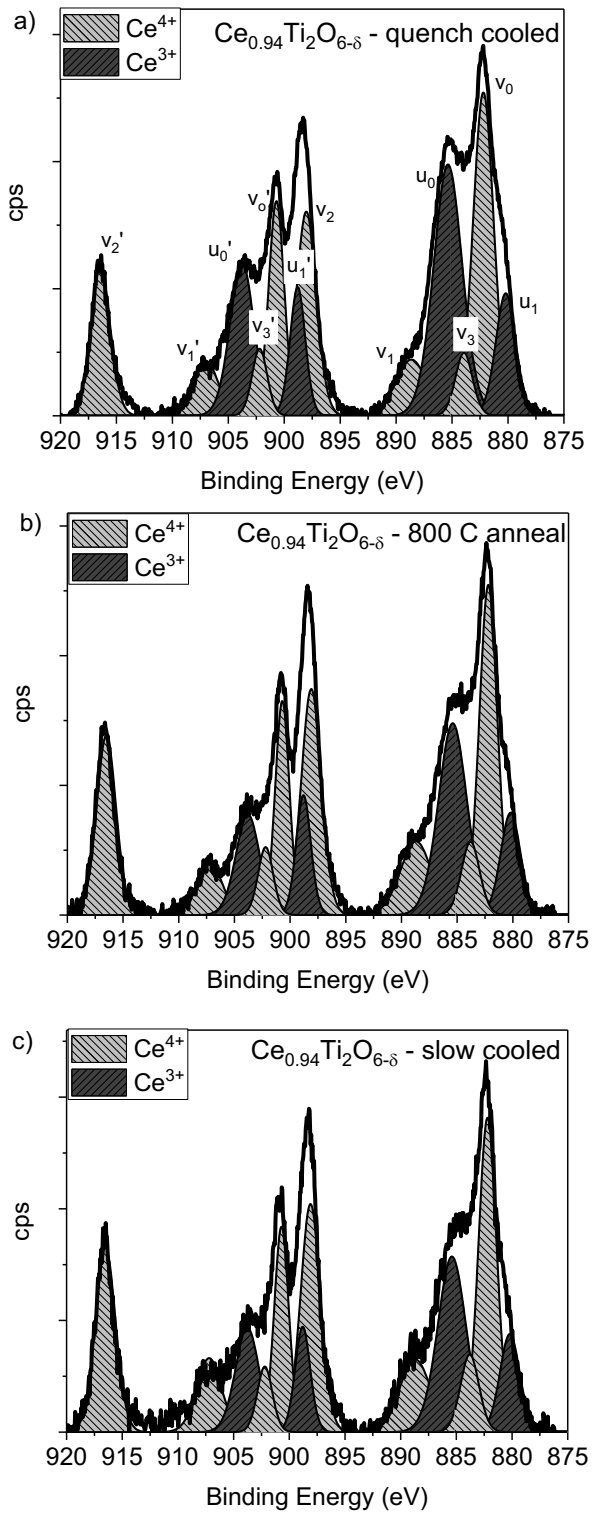
a)
Ce4+
Ce3+
Ce0.94Ti2O6-δ - quench cooled
v0
u0
vo'
v2
v2'
u0'
u1'
u1
v3'
v3
v1'
v1
cps
920 915 910 905 900 895 890 885 880 875
Binding Energy (eV)
b)
Ce4+
Ce3+
Ce0.94Ti2O6-δ - 800 C anneal
cps
920 915 910 905 900 895 890 885 880 875
Binding Energy (eV)
c)
Ce4+
Ce3+
Ce0.94Ti2O6-δ - slow cooled
cps
920 915 910 905 900 895 890 885 880 875
Binding Energy (eV)

Figure 7:

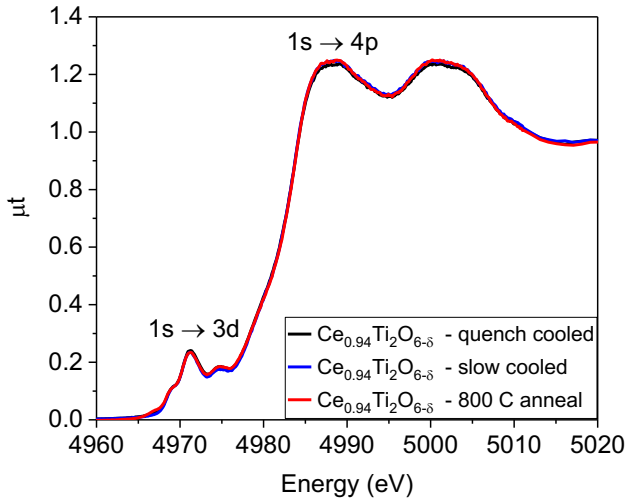
1s → 4p
1s → 3d
μt
Energy (eV)
1.4
1.2
1.0
0.8
0.6
0.4
0.2
0.0
4960
4970
4980
4990
5000
5010
5020
Ce0.94Ti2O6-δ - quench cooled
Ce0.94Ti2O6-δ - slow cooled
Ce0.94Ti2O6-δ - 800 C anneal

Figure 8:

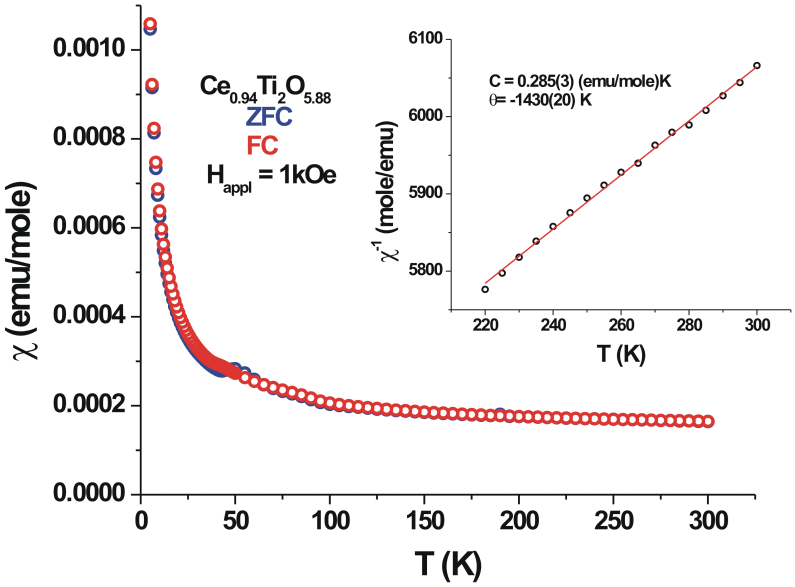
Ce0.94Ti2O5.88
ZFC
FC
Happl = 1kOe
χ (emu/mole)
T (K)
C = 0.285(3) (emu/mole)K
θ= -1430(20) K
χ-1 (mole/emu)
T (K)

Figure 9:

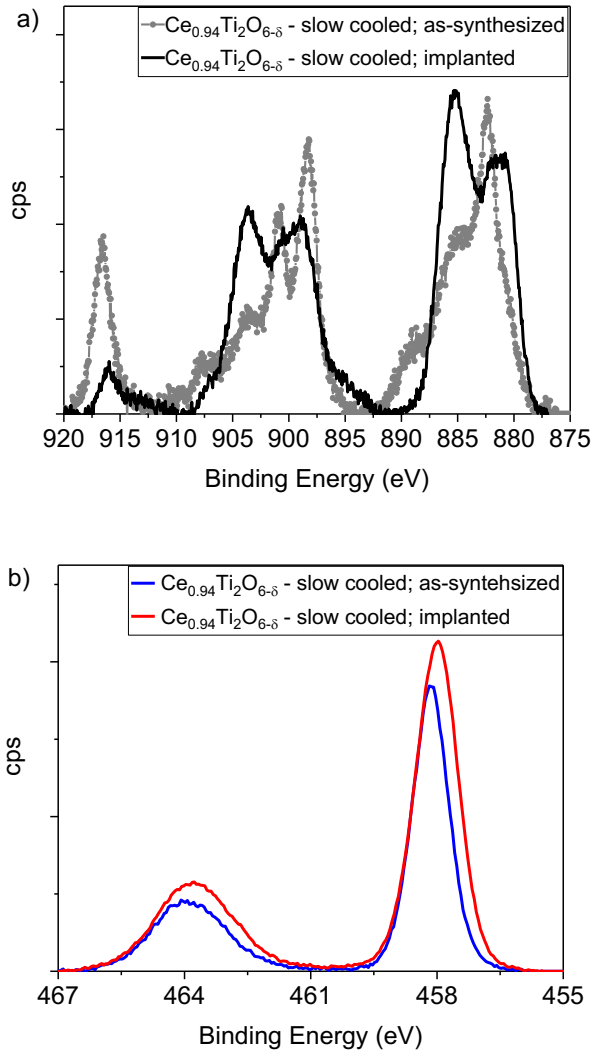
a)
$Ce_{0.94}Ti_2O_{6-\delta}$ - slow cooled; as-synthesized
$Ce_{0.94}Ti_2O_{6-\delta}$ - slow cooled; implanted
cps
920 915 910 905 900 895 890 885 880 875
Binding Energy (eV)
b)
$Ce_{0.94}Ti_2O_{6-\delta}$ - slow cooled; as-syntehsized
$Ce_{0.94}Ti_2O_{6-\delta}$ - slow cooled; implanted
cps
467 464 461 458 455
Binding Energy (eV)

Figure 10:

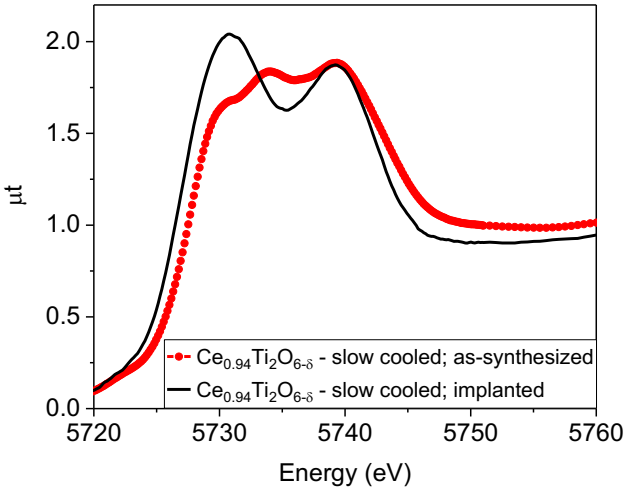
2.0
1.5
1.0
0.5
0.0
μt
5720
5730
5740
5750
5760
Energy (eV)
Ce0.94Ti2O6-δ - slow cooled; as-synthesized
Ce0.94Ti2O6-δ - slow cooled; implanted

Figure 11:

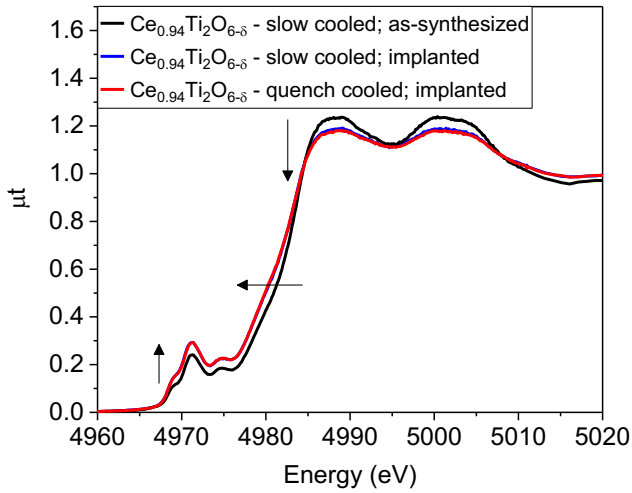
Ce0.94Ti2O6-δ - slow cooled; as-synthesized
Ce0.94Ti2O6-δ - slow cooled; implanted
Ce0.94Ti2O6-δ - quench cooled; implanted
μt
Energy (eV)
0.0
0.2
0.4
0.6
0.8
1.0
1.2
1.4
1.6
4960
4970
4980
4990
5000
5010
5020